

Copper (II) complexes of 3,5-di-*tert*-butyl-2-hydroxybenzoylhydrazones of 2-formylpyridine and 2-acetylpyridine, with tautomeric azine-scaffold-based architecture: Synthesis, crystal structures, the effect of counteranions on complexation, and their anti-microbial and anti-tuberculosis evaluation

Ganesh S. Hegde^{1,2}  | Sandeep P. Netalkar¹  | Vidyanand K. Revankar¹ 

¹Department of Chemistry, Karnatak University, Pavate Nagar, Dharwad 580 003, Karnataka, India

²Department of Chemistry, M. E. S., M. M. Arts & Science College, Sirsi, Uttara Kannada 581 402, Karnataka, India

Correspondence

V. K. Revankar, Department of Chemistry, Karnatak University, Pavate Nagar, Dharwad-580 003, Karnataka, India.
Email: vkrevankar@rediffmail.com

Funding information

Minor Research Project Program MRP(S)-0475/13-14/KAKA089/UGC-SWRO

A series of air- and moisture-stable copper (II) complexes of 3,5-di-*tert*-butyl-2-hydroxy-*N'*-(pyridin-2-ylmethylene)benzohydrazide (**L1H**) and 3,5-di-*tert*-butyl-2-hydroxy-*N'*-(1-(pyridin-2-yl)ethylidene)benzohydrazide (**L2H**) were synthesized. The two newly designed hydrazone Schiff base ligands with the tautomeric azine-scaffold involving N, N and O ligating architecture were derived from the condensation of 3,5-di-*tert*-butyl-2-hydroxybenzoylhydrazide with 2-formylpyridine and 2-acetylpyridine, respectively. The resultant ligands and their copper complexes were characterized using various spectro-analytical techniques, like infrared (IR), ¹H-NMR, ¹³C-NMR, electron paramagnetic resonance, electronic spectroscopy, thermogravimetric analysis and conductance measurements. The interesting inter-convertible *E/Z* geometrical isomeric forms of the ligand **L1H** was established by NMR and IR spectra. In addition, the molecular structures of **L2H**, **C3** and **C4** were unambiguously established using the single-crystal X-ray diffraction technique. The dichlorido-bridged dinuclear square pyramidal complexes, with the [Cu₂(μ-Cl)₂L₂] type of core units, were resulted for the complexes **C1** and **C3**, whereas z-in compressed mononuclear 1:2 (M:L) octahedral complex geometries resulted for **C2**, **C4** and the rest of the complexes even when various copper (II) precursor salts with different counteranions were used. The ligands and their complexes were investigated for the anti-microbial activities against gram-positive and gram-negative bacteria. The ligand **L2H** and its complexes **C3** and **C4** exhibited better anti-tuberculosis activity than the controls.

KEYWORDS

anti-microbial, anti-tuberculosis, azine-scaffold, copper complexes, single-crystal X-ray diffraction technique

1 | INTRODUCTION

The chemistry of hydrazones and their coordination compounds continues to receive much attention because hydrazides and their hydrazones can function as bioactive compounds.^[1] Among these, the aroyl hydrazones are the important and interesting series of hydrazone-derived ligands in the coordination chemistry, because of their ability to coordinate to the metal through the imine nitrogen as well as through the amide oxygen in either protonated or deprotonated form. An additional donor site can, however, be incorporated in the aroyl hydrazone ligands by carefully choosing such aldehydes or ketones that have donor atoms like nitrogen or oxygen at appropriate positions that can react with a hydrazide, forming the tridentate aroyl hydrazone Schiff bases. This flexibility of modifying the ligand design with appropriate additional donor atoms as well as the ease of its synthesis makes these ligands of considerable interest from the perspective of coordination geometry. Among the coordination complexes of hydrazones, copper (II) hydrazone complexes have received special attention primarily because of their structural diversity, redox and magnetic properties,^[2] which makes them potential candidates for use in catalysis as well as in biological applications.^[3–6] Copper being an important biologically significant metal, its hydrazone complexes show interesting biological properties, like, bacteriostatic activity,^[7] effective DNA binding,^[8] anti-microbial^[9] and anti-tuberculosis activities,^[10] etc. With tridentate ligands, Cu (II) can form both mononuclear and binuclear complexes depending on the stoichiometric reaction between the ligand and the metal ion. Commonly observed geometry is square pyramidal or distorted octahedral. The Cu (II) ion prefers distorted octahedral geometry when the stoichiometric reaction is 1:2 and square pyramidal with 1:1 stoichiometric reaction with respect to metal and ligand. However, the presence of the bridging group in the ligand may lead to binuclear complexes usually in square pyramidal complexes.

Inspired by the naturally occurring biologically significant metalloenzymes containing copper active sites, the present investigation was undertaken to study the nature of coordination modes of the aroyl hydrazone ligands with copper (II) salts. The two novel ligands 3,5-di-*tert*-butyl-2-hydroxy-*N'*-(1-(pyridin-2-yl)methylidene)benzohydrazide (**L1H**) and 3,5-di-*tert*-butyl-2-hydroxy-*N'*-(1-(pyridin-2-yl)ethylidene)benzohydrazide (**L2H**) were prepared, and their structural diversity with copper (II) ions while varying the counteranions is the focus of the current study. The complexes were also evaluated for anti-microbial and anti-tuberculosis activities.

2 | EXPERIMENTAL

2.1 | Materials and physical measurements

All the reagents used in this study were purchased from Sigma-Aldrich and used without further purification. The ¹H- and ¹³C-NMR spectra were recorded on AV400-Bruker 400 MHz High-Resolution Multinuclear FT-NMR Spectrometer and Agilent 400MR DD2 spectrometers, in CDCl₃ (¹H-NMR: 400 MHz; ¹³C-NMR: 100 MHz) at room temperature using TMS as an internal reference. Fourier transform-infrared (FT-IR) spectra were recorded in a KBr disc matrix using an Impact-410 Nicolet (USA) FT-IR spectrometer over the range of 4000–400 cm⁻¹. The mass spectra of the ligands were obtained on SHIMADZU GCMS-QP2010S. Electron paramagnetic resonance (EPR) spectra of copper (II) complexes were recorded on Varian E-4 X-band EPR spectrometer, using TCNE as the <g> marker. The electronic spectra were measured on a Hitachi 150–20 spectrophotometer over the range of 800–200 nm. Thermal analyses of the metal complexes were carried out on a Universal V2.4F TA instrument, keeping the final temperature at 1000°C and the heating rate at 10°C per min. The X-ray diffraction data were obtained at 296 K on Bruker X8 Proteum diffractometer. Intensity measurements were performed using monochromatic Cu-K α -radiation with $\lambda = 1.54178 \text{ \AA}$. Using Olex2,^[11] the structure was solved with the SIR2004^[12] structure solution program using Direct Methods and refined with the XH refinement package using CGLS minimization. Molecular graphics were generated using ORTEP-3, Mercury and Cameron.^[13–15]

2.2 | Synthesis of ligands (L1H and L2H)

3,5-di-*tert*-butyl-2-hydroxy-*N'*-(1-(pyridin-2-yl)methylidene)benzohydrazide (**L1H**) and 3,5-di-*tert*-butyl-2-hydroxy-*N'*-(1-(pyridin-2-yl)ethylidene)benzohydrazide (**L2H**)

The ligands **L1H** and **L2H** were prepared in three steps. First, the starting material, methyl 3,5-di-*tert*-butyl-2-hydroxybenzoate **1** was synthesized following the literature method.^[16] The ligand precursor 3,5-di-*tert*-butyl-2-hydroxybenzoylhydrazide **2** was synthesized by treating **1** with hydrazine hydrate following the common procedure as in Vogel,^[17] in the second step. The benzoyl hydrazone ligands were prepared in the third step as follows.

3,5-Di-*tert*-butyl-2-hydroxybenzoylhydrazide (**2**), 0.005 moles, in methanol (100 ml) was treated with 0.005 moles of pyridine-2-aldehyde for **L1H** and 2-acetylpyridine for

L2H taken in the round-bottom flasks separately. The reaction mixtures were stirred at room temperature for nearly an hour until the off-white precipitates resulted. The reaction products were then filtered off, dried and recrystallized from methanol resulting in the formation of ligands **L1H** and **L2H** with 80% yields in each case.^[18] Schematic representation of the syntheses of the ligands and numbering pattern for NMR assignment is given in Scheme 1.

L1H: yield: 80%; m.p.: 180°C; anal. calcd for C₂₁H₂₇N₃O₂ (%): C, 71.27; H, 7.65; N, 11.91. Found (%): C, 71.29; H, 7.69; N, 11.88. FT-IR (cm⁻¹): C=O (1683), pyridine C=N (1588), imine >C=N- (1630), OH (3427s), NH (3287), C-O (1253). ¹H-NMR (CDCl₃, 400 MHz): δ 15.63 (s, 1H, hydrazine NH), 12.64 (s, 1H, C(2)-phenolic OH), 8.73 (s, 1H, -HC=N), 7.45 (s, 1H, C4H, aromatic), 7.49 (s, 1H, C6H, aromatic), 8.04 (d, *J* = 8 Hz, 1H, C11H, aromatic), 7.67 (t, *J* = 7.6 Hz, 1H, C12H aromatic), 7.18 (t, *J* = 6 Hz, 1H, C13H aromatic), 8.46 (d, *J* = 15.6 Hz, 1H, C14H, aromatic), 2.48 (s, 3H, CH₃OH solvent). ¹³C-NMR (CDCl₃, 100 MHz, ppm): 148.9 (HC8 = N), 29.3, 31.3, 34.3, 35.2 (t Bu), 159.3 (-N=C7 = O), 152.6 (C2-OH phenolic), 112.0 (C1, aromatic), 138.1 and 138.0 (C3 and C5, aromatic), 124.5 and 124.3 (C4 and C6, aromatic), 140.2 (C10, aromatic), 121.5 (C11, aromatic), 136.9 (C12, aromatic), 129.7 (C13, aromatic), 138.8 (C14, aromatic), 169.2 (CH₃OH, solvent). UV-Vis (CHCl₃): λ_{max} (nm), (ε_{max} (Lmol⁻¹cm⁻¹)): 304 (4,765.3), 340 (2,942.8). *m/z*: 353.49.

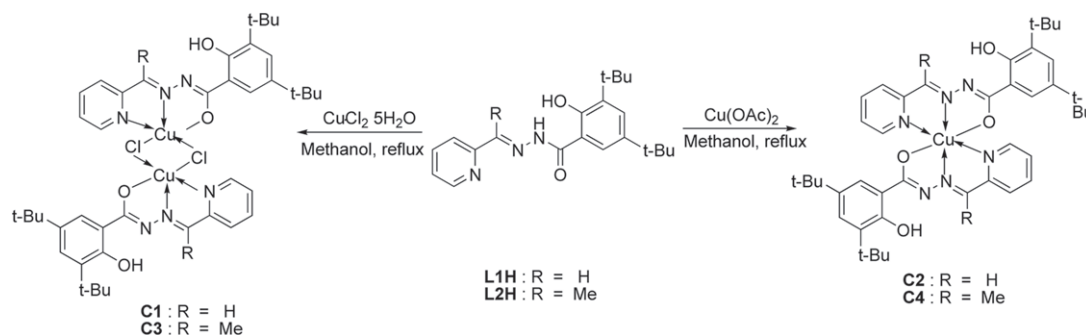
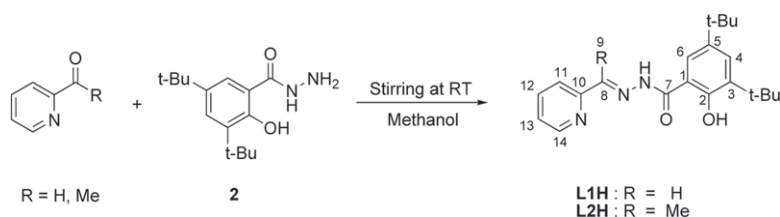
L2H: yield: 80%; m.p.: 185°C; anal. calcd for C₂₂H₂₉N₃O₂ (%): C, 71.86; H, 7.98; N, 11.45. Found (%): C, 71.84; H, 7.95; N, 11.43. FT-IR (cm⁻¹): C=O (1683),

pyridine C=N (1591), imine >C=N- (1631), OH (3426s), NH (3288), C-O (1278). ¹H-NMR (CDCl₃, 400 MHz): δ 15.94 (s, 1H, hydrazine NH), 12.80 (s, 1H, C(2)-phenolic OH), 7.52(d, *J* = 1.6 Hz, 1H, C4H, aromatic), 7.55 (d, *J* = 2 Hz 1H, C6H, aromatic), 7.68 (d, *J* = 8 Hz, 1H, C11H, aromatic), 7.96 (t, *J* = 8 Hz, 1H, C12H aromatic), 7.44 (t, *J* = 6.2 Hz, 1H, C13H aromatic), 8.76 (d, *J* = 4.8 Hz, 1H, C14H, aromatic). ¹³C-NMR (DMSO, ppm): 153.3 (HC8 = N), 29.3, 31.5, 34.3, 35.2 (t Bu), 168.7 (-N=C7 = O), 159.8 (C2-OH phenolic), 112.7 (C1, aromatic), 138.1 and 138.0 (C3 and C5, aromatic), 124.3 and 124.4 (C4 and C6, aromatic), 147.2 (C10, aromatic), 119.8 (C11, aromatic), 139.7 (C12, aromatic), 129.0 (C13, aromatic), 143.7 (C14, aromatic). UV-Vis (CHCl₃): λ_{max} (nm), (ε_{max} (Lmol⁻¹cm⁻¹)): 268 (4,558.0), 342 (6,531.4), *m/z*: 367.48.

2.3 | Synthesis of copper (II) complexes

The ligands **L1H/L2H** (2 mmol) and methanol (30 ml) were charged into a 100-ml round-bottom flask and allowed to warm with stirring in an oil bath maintained at 60–65°C. Hot methanolic solutions of copper (II) salts (1 mmol) were added to this dropwise with stirring. After the complete addition of metal salt solution, the reaction mixture was further refluxed for about 30–40 min at the same temperature. The isolated complexes were filtered in hot conditions, washed with hot ethanol and dried.^[19] The schematic route for the synthesis of Cu (II) complexes is presented in Scheme 2.

SCHEME 1 Synthetic route for the preparation of Schiff base ligands **L1H** and **L2H**



SCHEME 2 Synthetic route for the synthesis of the Cu (II) complexes, **C1**, **C2**, **C3** and **C4**

C1: yield: 65%; anal. calcd for $\text{Cu}_2\text{C}_{42}\text{H}_{52}\text{N}_6\text{O}_4\text{Cl}_2$ (%): C, 55.80; H, 5.82; N, 9.32. Found (%): C, 55.82; H, 5.80; N, 9.30. FT-IR (cm^{-1}): pyridine C=N (1563), >C=N-N=C < (1606), OH (3445), C-O (1247). Λ_M (CHCl_3 , $\text{mho cm}^2 \text{ mol}^{-1}$): 0.58. UV-Vis (CHCl_3): λ_{max} (nm), (ϵ_{max} ($\text{Lmol}^{-1}\text{cm}^{-1}$)): 280 (1,768.3), 390 (2,915.3), 414 (5774.9), 712 (73.22). EPR (g_{\parallel} , g_{\perp} , g_{av} , Grnd. State, Geometry): 2.129, 2.074, 2.0923, $d_{x^2-d_{y^2}}$, Sq. Pyramidal.

C2: yield: 70%; anal. calcd for $\text{CuC}_{42}\text{H}_{52}\text{N}_6\text{O}_4$ (%): C, 65.60; H, 6.85; N, 10.93. Found (%): C, 65.58; H, 6.82; N, 10.93. FT-IR (cm^{-1}): pyridine C=N (1560), >C=N-N=C < (1606), OH (3442), C-O (1253). Λ_M (CHCl_3 , $\text{mho cm}^2 \text{ mol}^{-1}$): 25.6. UV-Vis (CHCl_3): λ_{max} (nm), (ϵ_{max} ($\text{Lmol}^{-1}\text{cm}^{-1}$)): 254 (777.6), 288 (627.8), 415 (791.0), 675 (575.2), 715 (125.5). EPR (g_{\parallel} , g_{\perp} , g_{av} , Grnd. State, Geometry): 2.0476, 2.1434, 2.1115, d_{z^2} , Compressed Octahedral.

C3: yield: 80%; anal. calcd for $\text{Cu}_2\text{C}_{44}\text{H}_{56}\text{N}_6\text{O}_4\text{Cl}_2$ (%): C, 56.70; H, 6.08; N, 9.03. Found (%): C, 56.72; H, 6.06; N, 9.02. FT-IR (cm^{-1}): pyridine C=N (1568), >C=N-N=C < (1603), OH (3443), C-O (1246), Λ_M (CHCl_3 , $\text{mho cm}^2 \text{ mol}^{-1}$): 0.87. UV-Vis (CHCl_3): λ_{max} (nm), (ϵ_{max} ($\text{Lmol}^{-1}\text{cm}^{-1}$)): 288 (539.2), 393 (630.1), 414 (3844.0), 691 (98.76), 851 (30.55). EPR (g_{\parallel} , g_{\perp} , $g_{\text{av}}/g_{\text{iso}}$, Grnd. State, Geometry): 2.1748, 2.0759, 2.1089 (2.0823(RT)), $d_{x^2-d_{y^2}}$, Sq. Pyramidal.

C4: yield: 78%; m.p.: > 300°C; anal. calcd for $\text{CuC}_{44}\text{H}_{56}\text{N}_6\text{O}_4$ (%): C, 66.31; H, 7.07; N, 10.58. Found (%): C, 66.29; H, 7.08; N, 10.55. FT-IR (cm^{-1}): pyridine C=N (1568), >C=N-N=C < (1597), OH (3442), C-O (1251). Λ_M (CHCl_3 , $\text{mho cm}^2 \text{ mol}^{-1}$): 1.26. UV-Vis (CHCl_3): λ_{max} (nm), (ϵ_{max} ($\text{Lmol}^{-1}\text{cm}^{-1}$)): 253 (1410.8), 285 (1355.6), 383 (1850.4), 667 (266.93). EPR (g_{\parallel} , g_{\perp} , g_{av} , Grnd. State, Geometry): 2.0475, 2.1685, 2.1282, d_{z^2} , Compressed Octahedral.

3 | RESULTS AND DISCUSSION

3.1 | Synthesis and characterization

The synthetic protocol employed in the syntheses of the copper complexes **C1–C4** from the ligands **L1H** and **L2H** is outlined in Scheme 2. The reaction of 3,5-di-*tert*-butyl-2-hydroxybenzoylhydrazide with pyridine-2-aldehyde and 2-acetylpyridine formed the ligands **L1H** and **L2H**, respectively, in good yields. The ligands **L1H** and **L2H** on metallation reaction with copper (II) salts of different anions in methanol at room temperature yielded the Cu (II) complexes with the general formulae $[\text{Cu}_2\text{Cl}_2(\text{L1})_2]$ (**C1**), $[\text{Cu}(\text{L1})_2]$ (**C2**), $[\text{Cu}_2\text{Cl}_2(\text{L2})_2]$ (**C3**) and $[\text{Cu}(\text{L2})_2]$ (**C4**). Copper salts with various counteranions like chloride, acetate, nitrate, sulphate, phosphate and perchlorates were used to study their

effect on the complexation with the ligands. However, for both **L1H** and **L2H**, except chlorides, other anions did not enter the coordination sphere and all of them resulted in the same complex. Hence, only two distinct types of complexes for each ligand were considered for the elaborate study. The ligands **L1H** and **L2H** and their corresponding copper (II) complexes were soluble in common organic solvents like chloroform, dichloromethane, methanol, ethanol, acetonitrile, DMF and DMSO, etc. The yields of all the complexes were substantial. Slow evaporation of the ligand **L2H** in methanol and the complexes $[\text{Cu}_2\text{Cl}_2(\text{L2})_2]$ (**C3**) in methanol and $[\text{Cu}(\text{L2})_2]$ (**C4**) in chloroform resulted in the single crystals suitable for X-ray diffraction (XRD) studies. The stoichiometries of the metal ions and ligands were established by the metal estimations, CHN analysis and molar conductivity measurements. All the metal complexes melt above 300°C. The metal to ligand ratios for $[\text{Cu}_2\text{Cl}_2(\text{L1})_2]$ (**C1**) and $[\text{Cu}_2\text{Cl}_2(\text{L2})_2]$ (**C3**), i.e. Cu (II) complexes with copper chloride as metal precursors exhibited 2:2 molar ratios for metal:ligand, while the Cu (II) complexes prepared with copper acetate as metal precursors $[\text{Cu}(\text{L1})_2]$ (**C2**) and $[\text{Cu}(\text{L2})_2]$ (**C4**) exhibited 1:2 molar ratios for metal:ligand.

3.2 | Molar conductivity measurements

The molar conductance values of complexes in methanol and chloroform at concentration 10^{-3} M fall in the range 1–13 $\text{mho cm}^2 \text{ mol}^{-1}$ (Table 1). These values are much less than that expected for 1:1 electrolytes (65–90 $\text{mho cm}^2 \text{ mol}^{-1}$) and, hence, are feeble electrolytic in nature.^[20]

3.3 | NMR studies

^1H -NMR spectra of the common precursor of the ligands **L1H** and **L2H**, i.e. 3,5-di-*tert*-butyl-2-hydroxybenzoylhydrazide **2** shows the resonance of hydrazine-NH₂ proton at 3.85 ppm, -NH proton at 12.23 ppm, phenolic -OH proton at 8.1 ppm, aromatic protons

TABLE 1 Molar conductivity and electronic spectral data

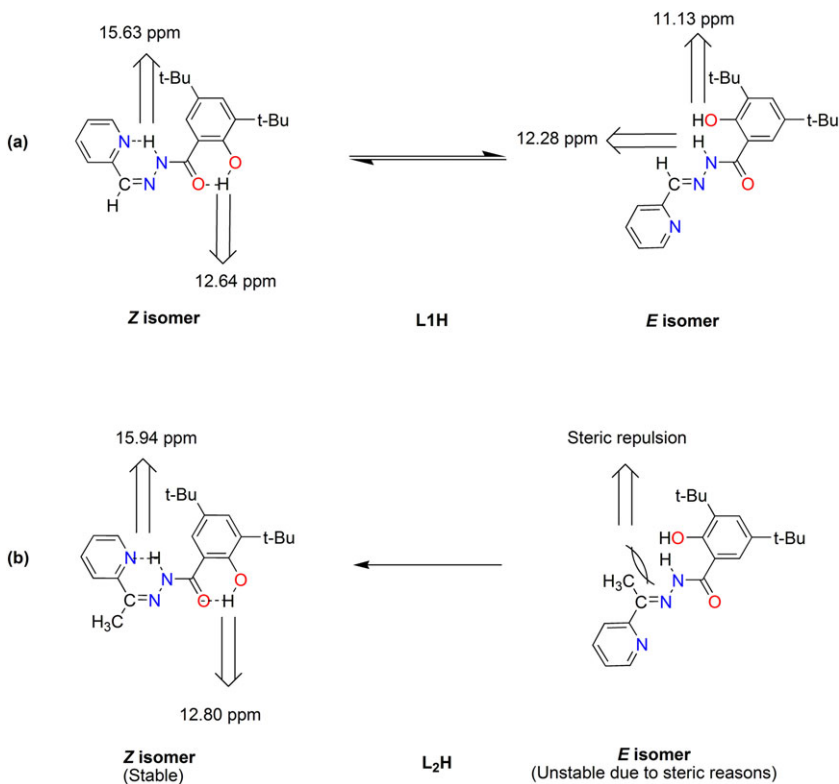
Compound	λ_{max} (nm)	Molar cond. Λ_M
L1H	211, 304, 340	–
C1	208, 280, 390, 414, 712	0.58
C2	210, 254, 288, 415, 675, 715	12.6
L2H	234, 268, 342	–
C3	234, 288, 393, 414, 691, 851	0.87
C4	253, 285, 383, 667	1.26

at 7.18 and 7.47 ppm, and tertiary butyl protons at 1.28 and 1.36 ppm, respectively. The other two precursors: pyridine-2-aldehyde and 2-acetylpyridine of ligand **L1H** and **L2H** exhibit a singlet at 10.1 ppm for an aldehydic proton and three proton singlets for acetyl protons at 2.729 ppm, respectively. These peaks shifted to 8.73 and 2.57 ppm in **L1H** and **L2H**, respectively, indicating the successful formation of Schiff base ligands through the imine linkage.^[21] ¹H-NMR spectra of the ligand **L1H** exhibited highly deshielded proton peaks at 15.63 and 12.64 ppm, and also some additional peaks even after using re-crystallized pure sample for the analysis. Careful investigation of the spectra of the compound and the literature survey^[22] concluded the presence of two inter-convertible *E/Z* geometrical isomers in the solution. There are two ways that the Schiff base ligand could be formed by imine linkage of the precursor **2** with 2-formylpyridine. Pyridine ring and the amide NH on the same side of the imine bond constitutes the *Z* isomer, and on the opposite side result in the *E* form.^[22,23] Interestingly, the *Z* isomer enables two intra-molecular hydrogen bonds, one between the pyridine nitrogen and the amide proton, and the other between the carbonyl oxygen of the amide and the phenolic hydrogen. The effect of these hydrogen bonds was reflected in the highly downfield peaks for amide NH and C(2)-OH at 15.63 and 12.64 ppm, respectively,^[24–26] whereas in the *E* isomer

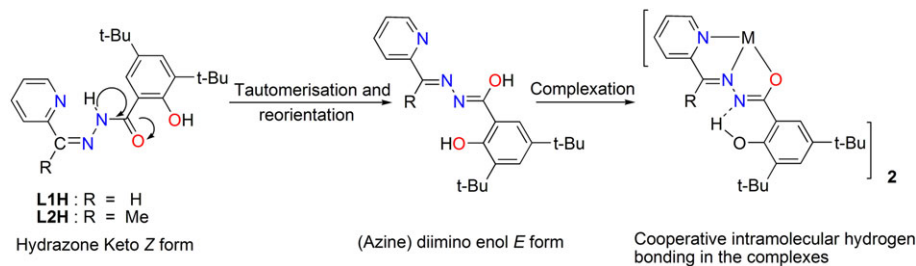
there is no scope for such hydrogen bonds, and these peaks were found at 12.28 and 11.13 ppm, respectively, as depicted in Scheme 3(a). (¹H-NMR spectra of ligand precursor **2** and both ligands are provided as Supporting information.) Further, the various additional peaks of low intensities also confirm the presence of both the mutually inter-convertible isomers in the solution state for **L1H**. The peaks due to NH and OH protons in the *Z* isomer appeared as sharp peaks in contrast to their usual broad nature. The probable reason for this would be the intra-molecular hydrogen bonding that checks their chemical exchangeability.

The ligand **L2H**, however, exhibits clear NMR spectrum without any additional peaks, due to the more stable *Z* isomer than the *E* isomer wherein steric repulsion between the bulky methyl group and the amidic proton dominates as depicted in Scheme 3(b). The downfield peaks at 15.94 and 12.80 ppm were authentically assignable again to the amide NH and phenolic C(2)-OH protons, respectively. (The above hypothesis is further supported by the X-ray crystal structure of the ligand **L2H** in the *Z* configuration, as detailed in Section 3.7.)

The aroyl hydrazone ligands **L1H** and **L2H** are potential NNO chelators, but the *Z* isomer is geometrically unfavourable for coordination with the metal ions, hence they must reorient to the *E* conformation during the complexation as shown in Scheme 4. The absence of any



SCHEME 3 Schematic representation of (a) inter-convertibility of *Z* and *E* isomers of **L1H** and (b) the steric repulsion in *E* isomer of **L2H** resulting in the more stable *Z* isomer and their corresponding ¹H-NMR shift of NH and OH protons



SCHEME 4 Schematic representation of the reorientation of ligands during complexation

additional small intensity peaks in $^1\text{H-NMR}$ spectra of the zinc (II) complexes of **L1H** as well as **L2H** also provided supporting evidence that the ligands **L1H** (*E/Z* isomeric mixture) and **L2H** (*Z* isomer) were all converted into the *E* isomeric form during the complexation ($^1\text{H-NMR}$ spectra of ligands and their zinc complexes were provided as Supporting information).

The $^{13}\text{C-NMR}$ spectrum of **L2H** was in agreement with the $^1\text{H-NMR}$ data, and all the signals were suitably assigned to the respective carbon atoms of the ligand molecule. However, $^{13}\text{C-NMR}$ spectra of **L1H**, like its proton NMR, was found to contain many additional peaks of low intensities making it difficult for the assignment. But, this observation further confirms the presence of both the *E/Z* geometrical isomers in the solution. Peaks at 149 and 153 ppm were due to $\text{RC}(8) = \text{N}$ azomethine carbon atoms in the ligands, respectively. The appearance of these two signals is the major supporting evidence for the successful formation of ligands **L1H** and **L2H**. The signals of $^{13}\text{C-NMR}$ spectra of **L1H** and **L2H** ligands observed at 159 and 169 ppm were assigned to the $-\text{HN-C}(7) = \text{O}$ carbon atoms in the two ligands, respectively. Other aromatic and aliphatic carbons were observed in the expected region, and are detailed in the Experimental section ($^{13}\text{C-NMR}$ spectra of ligand precursor **2**, ligands and their zinc complexes were provided as Supporting information).

3.4 | Infrared spectral studies

The FT-IR spectral data for the free ligands and their complexes are detailed in the Experimental section. The condensation of the aroyl hydrazide with 2-formyl pyridine/2-acetyl pyridine leading to the formation of the imine linking group and their coordination behaviour were supported in the IR spectral assignment. The FT-IR spectra of both the ligands exhibit typical intense bands centred at about 1630 cm^{-1} , which were assigned to azomethine functionality,^[27] and the peculiar $-\text{NH}$ bending absorption in the precursor **2** found at 1524 cm^{-1} is

completely absent in both the ligands,^[28,29] indicating the successful formation of the Schiff base ligands through the imine ($>\text{C}=\text{N}$) bond.

The IR spectral observation stands complementary with the NMR spectral interpretations. The presence of weak peaks at about 3288 and 1683 cm^{-1} in both the ligands were assigned to $>\text{NH}$ and $>\text{C}=\text{O}$ groups of the amide, respectively. The strong and sharp peaks at about 3426 cm^{-1} that appeared in both the ligands were assigned to the phenolic $-\text{OH}$ under the intra-molecular hydrogen bonding interaction with the carbonyl group of the amide.^[30,31] All these observations further support the *Z* isomeric forms of both the ligands in the solid state.

The *Z* isomeric hydrazone keto form of both the ligands in the solution undergoes rearrangement to the *E* conformation, followed by tautomerization to the diimino enol forms, in the presence of metal salts during complexation. Disappearance of the two amide bands in all the complexes confirms the transition to diimino enol tautomer in the complexes. The diimino enolic form of the ligand moieties in the complexes enjoys further stabilization through the cooperative intra-molecular hydrogen bonding between the uncoordinated diimine N with C2-OH , as depicted in Scheme 4.^[32] This observation was further supported by the fact that the sharp OH bands at about 3426 cm^{-1} in the ligands were broadened in all the complexes.

In order to satisfy the primary valency of the metal ion during the complexation, the ligands sacrifice the enolate proton to coordinate through enolate oxygen anion.^[33] The sharp azomethine $>\text{C}=\text{N}$ - bands at about 1630 cm^{-1} in both the ligands shifted to lower frequencies by about $25\text{--}30\text{ cm}^{-1}$ ^[34] in all the complexes, confirming the formation of azine group and coordination through one of its nitrogens.^[35] The bands at 1588 and 1591 cm^{-1} assigned to aromatic pyridine $\text{C}=\text{N}$ absorptions in both the ligands shift to a lower frequency by $10\text{--}15\text{ cm}^{-1}$ in all the complexes, suggesting complexation through this nitrogen.^[36] Hence, the IR spectra support the behaviour of both the ligands as tridentate; utilizing pyridine-N, azine-N and diimino enolate-O as donor sites.

The spectra are rather complex in the region below 500 cm^{-1} , where the various M-L bond stretching vibrations are often found in combination with other bands (the IR spectra of ligand precursor **2**, ligands and their complexes are provided in the Supporting information).

3.5 | Electronic spectral studies

The electronic spectra of the ligands and their copper complexes were recorded in chloroform, and the data are summarized in Table 1. Both the ligands exhibit UV-Vis absorption bands at about 211–230, 270–304 and 340–342 nm. The intense bands at about 211 and 234 nm in the ligands, which almost remain unchanged in the spectra of their complexes, were due to solvent absorptions. The ligand bands at about 270–304 and 340–342 nm were due to the $\pi \rightarrow \pi^*$ transitions of the organic moieties with various π systems.^[37,38] The ligands show broad and intense bands at about 304–342 nm that were assigned to $\pi \rightarrow \pi^*$ transition of azo $>\text{C}=\text{N}-\text{NH}$ -functional group.^[39] These bands in all the complexes exhibit red shift due to the tautomerization of azo to azine moiety $>\text{C}=\text{N}-\text{N}=\text{C}<$, and coordination of one of the azine nitrogens to the metal centres.

The electronic spectra of copper (II) complexes exhibited λ_{max} values at about 390, 414 and 690–712 nm in all the complexes, which were the electronic transitions influenced by the coordination bond. The electronic spectra of the copper complexes were observed as three main transitions. The spectra of the complexes also show moderate intense bands at $30\,000\text{--}35\,000\text{ cm}^{-1}$, assignable to nitrogen-centred ligand to metal charge transfer (LMCT) transitions from the coordinated unsaturated ligand to the metal ion.^[40] The bands at higher energies at about $\sim 30\,000\text{ cm}^{-1}$ are associated with the azomethine of azine group shifts to longer wavelength, indicating the coordination of azomethine nitrogen to copper.^[41] The ground state in an octahedral field is unstable due to the Jahn-Teller distortion; hence, ${}^2\text{E}_g$ of regular octahedral copper

(II) complexes cannot exist. The $t_{2g}e_g$ separation in a regular octahedral copper (II) complex varies from about $13\,000\text{ cm}^{-1}$ to about $18\,000\text{ cm}^{-1}$.

For the copper (II) complexes, **C2** and **C4** in chloroform (10^{-3} M solution), the d-d bands were observed in the regions 666–720 nm, i.e. $15\,000\text{--}13\,800\text{ cm}^{-1}$, which could be assigned to the ${}^2\text{T}_{2g}$ to ${}^2\text{E}_g$ transition of an octahedral geometry. However, the ${}^2\text{T}_{2g}$ to ${}^2\text{E}_g$ states of the octahedral Cu (II) ion (d^9) split under the influence of the tetragonal distortion, and the three transitions ${}^2\text{B}_{1g}{}^2\text{E}_g$, ${}^2\text{B}_{1g}{}^2\text{B}_{2g}$ and ${}^2\text{B}_{1g}{}^2\text{A}_{1g}$ are expected.^[42] But, such complexes exhibit^[43] a broad band with or without the shoulder between 500 and 770 nm depending upon the strength of the in-plane and axial ligands. It is concluded that all the three transitions will be within this broad envelope. The spectra of copper (II) complexes **C2** and **C4** exhibit broad d-d absorption bands with λ_{max} at 675 and 667 nm ($14\,815$, $14\,992\text{ cm}^{-1}$), with ϵ_{max} values of 575.2 and 266.93 indicative of a distorted octahedral system.^[44]

Broad asymmetric peaks at about 712 nm, with a low-energy shoulder band, have been observed for Schiff base binuclear copper (II) complexes with square-pyramidal geometries.^[45–47] The bridged di-copper bivalent complexes generally show an LMCT band in the near-UV region at about 414 nm^[48,49] with ϵ_{max} values of 5774.9 3844.0 for $[\text{Cu}_2\text{Cl}_2(\text{L1})_2]$ (**C1**) and $[\text{Cu}_2\text{Cl}_2(\text{L2})_2]$ (**C3**) complexes, which were assigned with the square pyramidal geometry.^[50] The representative spectra of ligand **L2H** and complex **C3** are shown in Figure 1. The remaining UV-Vis spectra are provided in the Supporting information.

3.6 | EPR spectral studies

The EPR spectra are recorded for copper complexes in powder form, and the results are given in Table 2. $\text{G} = 2.303$ for the dimeric complex **C3**, the value of which is less than 4 hence, a considerable exchange interaction is

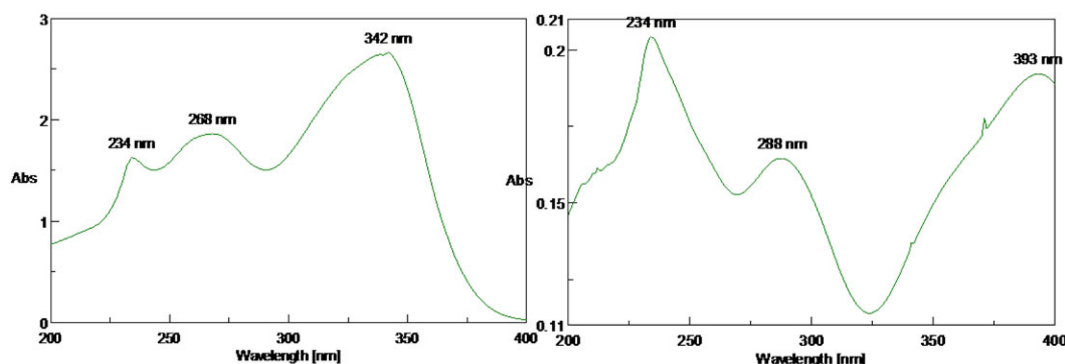


FIGURE 1 Representative electronic spectrum of ligand **L2H** and its complex **C3**

TABLE 2 EPR data

Comp.	g_{\parallel}	g_{\perp}	g_{av}/g_{iso}	μ	Ground state	Geometry
C1	2.129	2.074	2.0923	1.812	$d_{x^2-y^2}$	Square pyramidal
C2	2.0476	2.1434	2.1115	1.829	d_{z^2}	Compressed octahedral
C3	2.1748	2.0759	2.1089	1.826	$d_{x^2-y^2}$	Square pyramidal
C3	–	–	2.0823(RT)	1.803	$d_{x^2-y^2}$	Square pyramidal
C4	2.0475	2.1685	2.1282	1.843	d_{z^2}	Compressed octahedral

indicated in this solid complex. The g_{\parallel} is the moderately sensitive function of the metal–ligand covalency.^[51] The ionic environment is indicated when g_{\parallel} is 2.3 or larger, and it is less than 2.3 for more covalent environments. The ground state orbital and the respective geometry for all the complexes were tabulated based on the corresponding ‘g’ values. The g_{\parallel} values < 2.3 for all the copper complexes indicate the larger percentage of covalency in their metal–ligand bonds. The shape of the EPR graph indicates that these complexes may have either a square pyramidal or elongated octahedral geometry. The lowest g_{av} value of **C1** and **C3** compared with other complexes is attributed to the bis μ chloro bridge present in these bimetallic square pyramidal complexes. The **C3** complex showed g_{iso} , when the spectrum was taken for the sample in the powdered form at room temperature. However, the spectrum taken at 77 K for this complex dissolved in DMSO appears to exhibit anisotropy with the two ‘g’ values, as depicted in Figure 2. A similar observation was recorded by Roy *et al.*^[52]

The X-band EPR spectrum of **C4** was found to be of the inverse type, and the z-in compressed octahedral geometry was assigned based on the ‘g’ values, as well

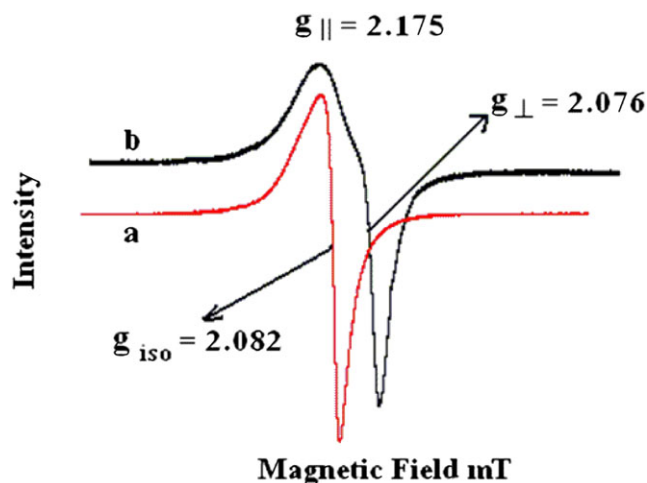


FIGURE 2 X-band electron paramagnetic resonance (EPR) spectrum of complex **C3** (a) in the solid state at room temperature, and (b) in DMSO solution at 77K

as from the single-crystal XRD analysis. The ligation of **L2H** was tried with copper salts of various anions like chloride, acetate, nitrate, perchlorate, phosphate and sulphate to look for the subsequent effect on complexation. The chloride salt exhibited a normal EPR spectrum; however, acetate and all other salts exhibited the compressed octahedral geometry. The EPR spectra of all of them appear similar with the same g_{\parallel} , g_{\perp} and g_{av} values, so as their IR spectra also overlap with each other. This was the clear indication that anionic species other than chloride neither entered the coordination sphere, nor in any way were retained in the complex compound. Thus, this indicated no role of them in the coordination (the EPR spectra of the complexes are provided in the Supporting information).

3.7 | Thermal analysis

All the complexes were studied for their thermal behaviour over the temperature range of 25–1000°C under ambient atmosphere (the thermograms of the ligands and the representative complexes were provided as Supporting information).

Thermal studies of both the ligands showed weight loss in the temperature range of 130–150°C amounting to 2.3–5.7% due to the loss of lattice-held methanol molecules. Further, both the ligands were thermally stable up to about 270°C, and then **L1H** and **L2H** underwent complete degradation within 400°C and 500°C, respectively.

Thermal studies of **C1** indicated that the complex was stable up to 273°C after the loss of lattice-held solvent molecule during 37–65°C amounting to 6.7%. The observed weight loss of 82.4% from 273 to 307°C corresponds to the loss of arolydrazone ligand fragment ($C_{42}H_{52}N_6O_4Cl^{3-}$). The remaining part Cu_2Cl^{3+} gradually loses chlorine and finally oxidized to cupric oxide from 307 to 1000°C. The thermal studies of **C2** indicated that the complex was very stable up to 354°C. Then the thermogram exhibited sharp weight loss of 79.2% up to 366°C due to the loss of two ligand fragments ($C_{42}H_{52}N_2$). Finally, the remaining fragment $CuN_4O_2^{3-}$

decomposed to stable cupric oxide. The thermogram of complex **C3** indicated the weight loss of 2.7% from 49 to 72°C indicating the loss of lattice-held solvent molecule, and then the complex was stable up to 317°C. The weight loss of 76.9% from 317 to 329°C amounts to the loss of coordinated ligand part ($C_{44}H_{56}N_6O_4^{2-}$), leaving behind the $Cu_2Cl_2^{2+}$ fragment. Then from 329°C onwards, the thermogram showed gradual weight loss due to chlorine molecule, and the formation of stable refractory copper oxide compound. The thermogram curve for **C4** indicated stability up to 273°C, and then decomposed in three sharp intermediate steps. The weight loss of 41.9% in the first step from 273 to 276°C is near to the calculated mass loss of one of the coordinated ligand fragments ($C_{22}H_{28}N_3$), leaving two oxygen atoms intact with the remaining part. In the second step, the weight loss of

39% amounted to another ligand fragment of $C_{22}H_{28}$. The remaining metal fragment of CuN_2O_4 gradually decomposed to the stable copper oxide as exhibited by the plateau.

3.8 | Single-crystal X-ray diffraction studies

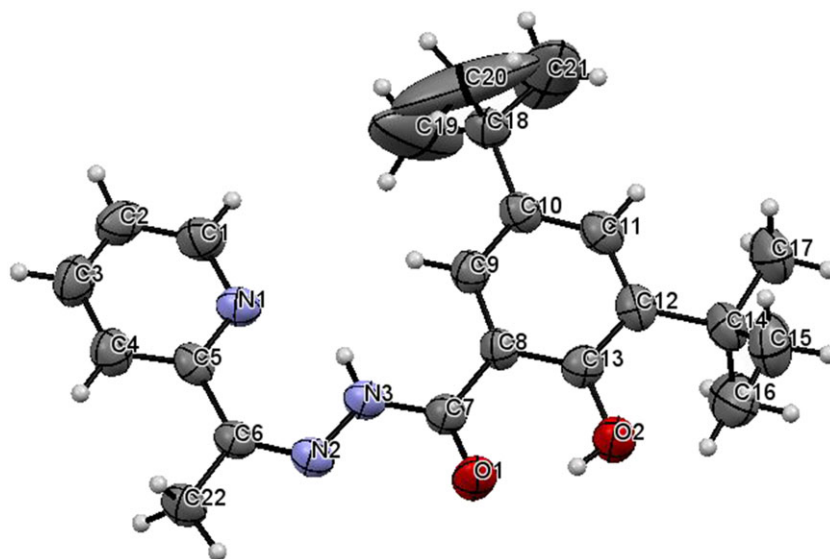
The structures of the ligand **L2H** and its copper complexes **C3** and **C4** were unambiguously established by the XRD studies. Summaries of the crystallographic data, bond lengths and bond angles of the compounds **L2H**, **C3** and **C4** are shown in Tables 3 and 4. ORTEP representations of **L2H**, **C3** and **C4** showing 50% displacement ellipsoids are shown in Figures 3, 4 and 5, respectively.

TABLE 3 Crystal data and structure refinement details of the ligand **L2H** and the complexes, **C3** and **C4**

Crystal data	L2H	C3	C4
Empirical formula	$C_{22}H_{29}N_3O_2$	$C_{44}H_{56}Cl_2Cu_2N_6O_4$	$C_{44}H_{56}CuN_6O_4$
Formula weight	367.49	930.96	796.49
Temperature/K	293	293(2)	296(2)
Crystal system	Orthorhombic	Monoclinic	Orthorhombic
Space group	<i>Pbca</i>	<i>P2₁/c</i>	<i>Pnna</i>
<i>a</i> /Å	8.3683(15)	16.2026(7)	10.4172(7)
<i>b</i> /Å	15.211(3)	9.5114(5)	33.818(3)
<i>c</i> /Å	33.321(6)	15.7038(7)	12.0400(9)
α /°	90.00	90.00	90.00
β /°	90.00	113.256(2)	90.00
γ /°	90.00	90.00	90.00
Volume/Å ³	4241.6(7)	2223.47(10)	4241.6(6)
<i>Z</i>	8	2	4
$\rho_{\text{calc}}/\text{cm}^3$	1.151	1.390	1.247
μ/mm^{-1}	0.07	2.668	1.11
<i>F</i> (000)	1584	972.0	1692.0
Crystal size/mm ³	0.24 × 0.21 × 0.18	0.29 × 0.25 × 0.22	0.23 × 0.11 × 0.09
Radiation	MoK α ($\lambda = 0.71070$ Å)	CuK α ($\lambda = 1.54178$ Å)	CuK α ($\lambda = 1.54178$ Å)
2 θ range for data collection/°	4.88 to 47.7	12.0 to 129.0	11.6 to 128.8
Index ranges	$-9 \leq h \leq 9, -17 \leq k \leq 17,$ $-37 \leq l \leq 37$	$-17 \leq h \leq 18, -11 \leq k \leq 11,$ $-18 \leq l \leq 18$	$-11 \leq h \leq 11, -39 \leq k \leq 39,$ $-13 \leq l \leq 13$
Reflections collected	14 321	13 513	20 099
Independent reflections	3273 ($R_{\text{int}} = 0.036$)	3651 ($R_{\text{int}} = 0.039$)	3483 ($R_{\text{int}} = 0.145$)
Data/restraints/parameters	1882/0/1	3651/0/269	3483/0/288
Goodness-of-fit on F^2	0.72	1.05	1.04
Final <i>R</i> indexes [$I \geq 2\sigma(I)$]	$R_1 = 0.036, wR_2 = 0.148$	$R_1 = 0.039, wR_2 = 0.101$	$R_1 = 0.066, wR_2 = 0.202$
Final <i>R</i> indexes (all data)	$R_1 = 0.036, wR_2 = 0.148$	$R_1 = 0.039, wR_2 = 0.101$	$R_1 = 0.1079, wR_2 = 0.2021$
Largest diff. peak/hole/e Å ⁻³	0.79/−0.30	0.54/−0.46	0.36/−0.49

TABLE 4 Selected bond lengths (Å) and angles (°) of complexes C3 and C4

L2H		C3		C4	
Bond lengths (Å)		Bond lengths (Å)		Bond lengths (Å)	
C6-N2	1.2963(1)	Cu1-N2	1.926(2)	Cu1-N2 ¹	1.963(3)
C5-N1	1.3553(2)	Cu1-O1	1.971(16)	Cu1-N2	1.963(3)
C5-C6	1.4845(2)	Cu1-N1	2.015(2)	Cu1-O1 ¹	2.147(3)
C1-N1	1.3261(2)	Cu1-Cl1	2.2216(6)	Cu1-N1	2.185(4)
N2-N3	1.3771(2)	Cu1-Cl1 ¹	2.7446(6)	O1-C7	1.263(5)
N3-H30	0.880	O1-C7	1.280(3)	N3-C7	1.344(5)
C7-O1	1.2385(2)	N1-C1	1.338(3)	N3-N2	1.373(5)
C13-O2	1.3502(2)	N1-C5	1.363(3)	C8-C7	1.476(6)
Bond angles (°)		Bond angles (°)		Bond angles (°)	
C6-N2-N3	117.893(11)	N2-Cu1-O1	80.02(7)	N2 ¹ Cu1N2	174.9(2)
N3-C7-C8	116.190(10)	N2-Cu1-N1	80.17(8)	N2 ¹ Cu1O1	100.07(13)
C7-C8-C13	118.195(9)	O1-Cu1-N1	159.52(8)	O1 ¹ Cu1O1	97.62(17)
C8-C7-N3	116.190(10)	N2-Cu1-Cl1	174.10(6)	N2Cu1N1	77.08(14)
H30-N3-C7	121.8	O1-Cu1-Cl1	99.56(5)	C7O1Cu1	109.7(3)
C7-C8-C9	122.855(8)	N1-Cu1-Cl1	99.60(6)	C1N1C5	119.8(4)
C9-C10-C18	121.145(8)	N1-C1-C2	121.9(2)	N3C7C8	116.0(4)

**FIGURE 3** ORTEP projection of **L2H** showing 50% probability ellipsoids

The asymmetric unit of **L2H** crystallized in an orthorhombic crystal system with no crystal-held solvent or water molecules. The ligand structure maintains overall co-planarity with only the *t*-butyl group popping out of the plane of the molecule. With respect to the azomethine module (C6 = N2), which averages to 1.294(5) Å, the configuration is *Z*, with the highest priority groups, pyridine and the amide functionality in the *cis*-arrangement, that is on the same side of this azomethine linkage. This configuration is stabilized by the strong intra-molecular

hydrogen bonding interaction between pyridine nitrogen, N1 and the proton of amidic linkage H30, N3-H30... N1, N3-H30 averaging to 2.616 Å and H31...N1 averaging to 1.913 Å. The O2-H20...O1 hydrogen bonding is characterized by O2-H20 length of 0.82 Å and H20...O1 length averaging to 1.76 Å.

The X-ray structure of complex **C3** shows that two square planar copper (II) centres, joined by the two bridging chloride ions in an end-to-end fashion, share the axial and equatorial positions, respectively.^[53] Both the metal

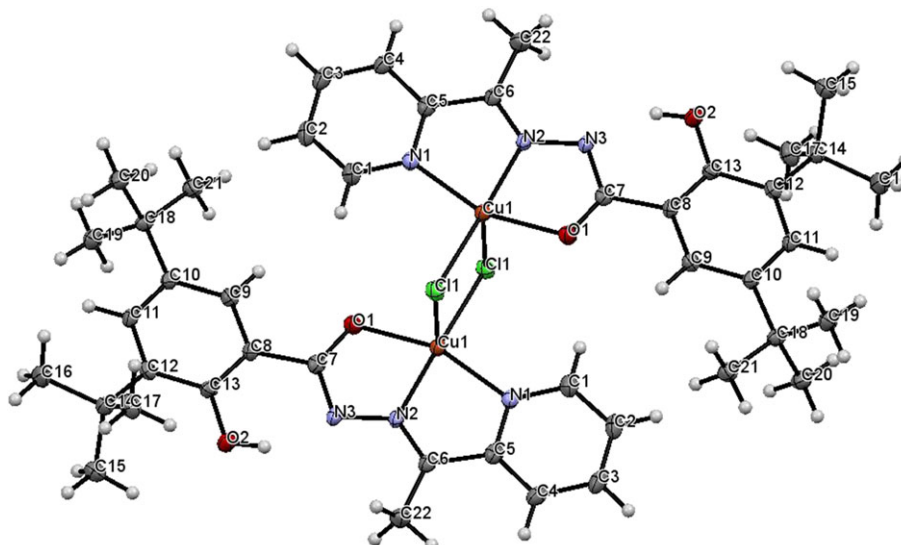


FIGURE 4 ORTEP projection of **C3** showing 50% probability ellipsoids

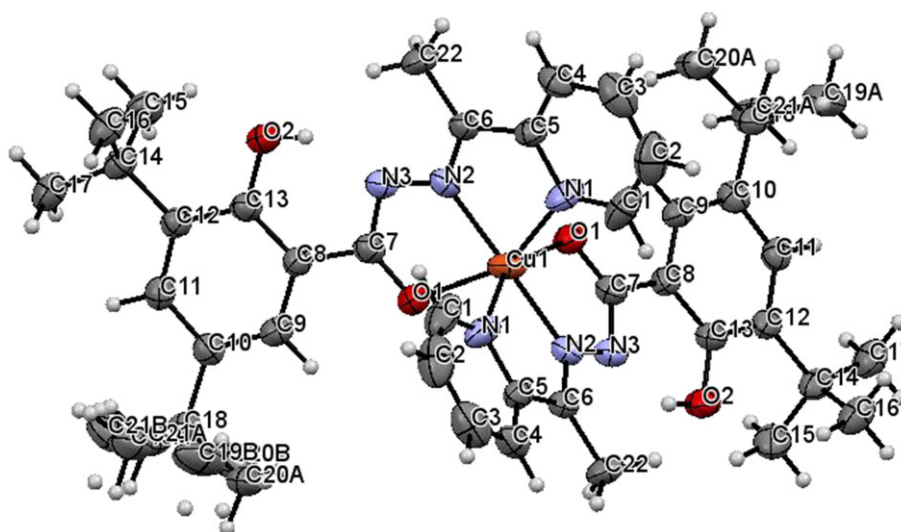


FIGURE 5 ORTEP projection of **C4** showing 50% probability ellipsoids

centres have penta coordination with the distorted square pyramidal geometry using an N_2OCl_2 coordination sphere provided by a tridentate ligand in a meridional fashion with a dihedral angle of 88.64° , using pyridine-N, azine-N and diimino enolate-O and two bridging chloride ions, respectively. The NNO donor sites of the tridentate ligand coordinate the Cu (II) centres to form two five-membered C_2N_2Cu and CN_2OCu chelate rings, with bite angles of $80.17(8)^\circ$ and $80.02(7)^\circ$, respectively, in both halves of the complex. The deviation of both Cu(1) atoms from the coordinate plane [the least squares plane composed of Cl(1), O(1), N(2) and N(1)] is 0.107 \AA . The Cu1...Cu1 distance is $3.45(5) \text{ \AA}$. The equatorial Cu1–

Cl1 [$2.2216(6) \text{ \AA}$] distance is much smaller than the axial Cu1–Cl2 [$2.7446(6) \text{ \AA}$] distance, clearly indicating the distorted as well as compressed square pyramidal geometry around the metal centre. The equatorial Cu1–Cl1 [$2.2216(6) \text{ \AA}$] bond distance around both the metal centres is comparable to those of similarly reported complexes,^[54] but this distance is longer than Cu1–N1 [$2.015(2) \text{ \AA}$], Cu1–N2 [$1.926(2) \text{ \AA}$] and Cu1–O1 [$1.9710(16) \text{ \AA}$]. The Cu1–Cl2–Cu2 angle is found to be $87.40(2)^\circ$.

The X-ray structure of complex **C4** shows a distorted octahedral structure wherein the Cu (II) metal ion centre is surrounded by an N_4O_2 coordination sphere, provided

by a tridentate ligand in a meridional fashion with a dihedral angle of 88.74° using pyridine-N, azine-N and diimino enolate-O as donor sites. The NNO donor sites of the tridentate ligand coordinate the Cu (II) centre to form two five-membered C₂N₂Cu and CuN₂CO chelate rings, with bite angles of 77.08(14)° and 76.53(12)°, respectively, indicating distortion from an ideal octahedral geometry. The metal centre is sited in an axially distorted compressed octahedral geometry; probably due to Jahn–Teller distortion. The C–O bond distance of 1.263(5) Å supports the existence of coordination via enolate oxygen to the metal centre. The Cu–N (py) bond and Cu–O(1) (carboxyl) bonds [2.185(4) Å and 2.147(3) Å] are significantly longer than the Cu–N(2) [1.963(3) Å], although the latter is formed via deprotonation. This difference can be attributed by the bis (chelating) mode of the ligand in which the Cu–N/O bonds (pyridine nitrogen) and carbonyl oxygen (O-carboxyl) appear to be shared by two five-membered chelate rings. Similar observations were seen in the complexes having similar coordination mode.^[55] In the extended crystal structures of both the complexes, the azine (diimino) enol tautomeric form of the ligand is further supported by the existence of cooperative intramolecular hydrogen bonding between azine nitrogen and hydroxyl -OH group.

All the crystal structures were deposited to Cambridge Crystallographic Data Centre via the joint CCDC/FIZ Karlsruhe deposition service. The crystal structures of the ligands **L2H** [Cu₂Cl₂(L2)₂] (**C3**) and [Cu(L2)₂] (**C4**) were assigned the CCDC numbers as 1884153, 1867982

and 1867983, respectively. The supplementary crystallographic data of these compounds can be obtained free of charge via <https://www.ccdc.cam.ac.uk/structures/>.

3.9 | Biological assay

All the synthesized compounds were evaluated for their antimicrobial activity against *Staphylococcus aureus*, a gram-positive bacterium, and gram-negative *Escherichia coli* pathogens using micro-broth dilution method. *Ciprofloxacin* is used as the standard drug to compare the activity of the samples and the minimum inhibitory concentration (MIC) of which for both the pathogens is 2 µg mL⁻¹. The potency of ligands and their complexes was studied by comparing the turbidity^[56] formed with that of the standard drug on two bacterial strains, and the result is shown in Table 5. The ligand **L2H** and all its copper complexes exhibited better activity even than the 'Ciprofloxacin' control for the *S. aureus* microorganism. However, for *E. coli*, except complex **C3**, the rest of the compounds were better than the control.

The ligand **L1H** in the *E/Z* isomeric forms and its complexes showed different antimicrobial behaviour against gram-positive and gram-negative bacteria, respectively. **L1H** and **C1** were sensitive to *S. aureus*, only at higher concentrations, i.e. at 12.5 and 25 µg mL⁻¹, respectively, whereas **C2** was sensitive at 0.8 µg mL⁻¹ concentration. However, **L1H** and both of its complexes were very sensitive to *E. coli* at very low concentration of 0.4 µg mL⁻¹.

TABLE 5 Antimicrobial activity report

Sl. no.	Samples	100 µg mL ⁻¹	50 µg mL ⁻¹	25 µg mL ⁻¹	12.5 µg mL ⁻¹	6.25 µg mL ⁻¹	3.12 µg mL ⁻¹	1.6 µg mL ⁻¹	0.8 µg mL ⁻¹	0.4 µg mL ⁻¹	0.2 µg mL ⁻¹
<i>Staphylococcus aureus</i>											
1	L1H	S	S	S	S	R	R	R	R	R	R
2	C1	S	S	S	R	R	R	R	R	R	R
3	C2	S	S	S	S	S	S	S	S	R	R
4	L2H	S	S	S	S	S	S	S	S	S	R
5	C3	S	S	S	S	S	S	S	S	S	R
6	C4	S	S	S	S	S	S	S	S	S	R
<i>Escherichia coli</i>											
1	L1H	S	S	S	S	S	S	S	S	S	R
2	C1	S	S	S	S	S	S	S	S	S	R
3	C2	S	S	S	S	S	S	S	S	S	R
4	L2H	S	S	S	S	S	S	S	S	S	R
5	C3	S	S	S	S	S	S	R	R	R	R
6	C4	S	S	S	S	S	S	S	S	S	R

S, Sensitive; R, Resistant.

TABLE 6 Anti-tuberculosis activity report

Sl. no.	Samples	100 $\mu\text{g mL}^{-1}$	50 $\mu\text{g mL}^{-1}$	25 $\mu\text{g mL}^{-1}$	12.5 $\mu\text{g mL}^{-1}$	6.25 $\mu\text{g mL}^{-1}$	3.12 $\mu\text{g mL}^{-1}$	1.6 $\mu\text{g mL}^{-1}$	0.8 $\mu\text{g mL}^{-1}$
1	L1H	S	R	R	R	R	R	R	R
2	C1	S	S	S	S	R	R	R	R
3	C2	S	S	S	R	R	R	R	R
4	L2H	S	S	S	S	S	S	R	R
5	C3	S	S	S	S	S	S	S	R
6	C4	S	S	S	S	S	S	R	R

S, Sensitive; R, Resistant.

The synthesized compounds were also evaluated for their anti-mycobacterial activities against *Mycobacterium tuberculosis* (H37 RV strain): ATCC No-27294, using the Microplate Alamar Blue Assay (MABA) method.^[57] The results of the analysis were shown in Table 6. The MIC of ligand **L2H** was found to be $3.125 \mu\text{g mL}^{-1}$ and is as good as three controls, i.e. pyrazinamide ($3.125 \mu\text{g mL}^{-1}$), ciprofloxacin ($3.125 \mu\text{g mL}^{-1}$) and streptomycin ($6.25 \mu\text{g mL}^{-1}$). The MIC value of $1.6 \mu\text{g mL}^{-1}$ for **C3** and $3.125 \mu\text{g mL}^{-1}$ for **C4**, which are almost four and two times more active than standard streptomycin ($6.25 \mu\text{g mL}^{-1}$) and two times more active than and as active as the pyrazinamide and ciprofloxacin ($3.125 \mu\text{g mL}^{-1}$ each) standards, respectively.

The MIC values of **L1H** and its complexes were again different from others, as neither the ligand nor its complexes **C1** and **C2** exhibited better sensitivity against *M. tuberculosis*. The ligand was sensitive only at very high concentration of $100 \mu\text{g mL}^{-1}$, whereas the complexes **C1** and **C2**, even though they exhibited better sensitivities than ligand, they were not better than any of the three standard controls.

4 | CONCLUSION

The copper (II) complexes of two new ligands **L1H** and **L2H**: 3,5-di-*tert*-butyl-2-hydroxybenzoylhydrazones of 2-formylpyridine and 2-acetylpyridine were synthesized in good yields. The ligand **L1H** exists as inter-convertible *E/Z* geometric isomeric forms, whereas the ligand **L2H** exists exclusively as a *Z* isomer due to steric reasons. But both the ligands **L1H** and **L2H** undergo transformation to the *E* form in order to coordinate to the Cu metal centre. Further, the ligands bind the Cu (II) ion through the pyridine-N, azine-N and diimide enolate-O coordination sites in the tridentate manner. The various spectro-analytical techniques, in addition to the single-crystal X-ray diffraction studies, assisted in deciding the molecular structures of the copper complexes indicating the 2:2

(M:L) stoichiometry for $[\text{Cu}_2\text{Cl}_2(\text{L1})_2]$ (**C1**) and $[\text{Cu}_2\text{Cl}_2(\text{L2})_2]$ (**C3**), and 1:2 for $[\text{Cu}(\text{L1})_2]$ (**C2**) and $[\text{Cu}(\text{L2})_2]$ (**C4**). Thus, from the physico-chemical investigation, it was observed that the coordination mode of the ligands was of mono basic tridentate in all the complexes. The two distinct dichlorido-bridged dinuclear copper (II) complexes, i.e. $[\text{Cu}_2\text{Cl}_2(\text{L1})_2]$ (**C1**) and $[\text{Cu}_2\text{Cl}_2(\text{L2})_2]$ (**C3**) adopted distorted square pyramidal geometries. However, the complexes derived from Cu (II) acetate precursors, i.e. $[\text{Cu}(\text{L1})_2]$ (**C2**) and $[\text{Cu}(\text{L2})_2]$ (**C4**) adopted the six coordinated distorted octahedral geometries.




Although the copper (II) precursors with various counter ions like chloride, acetate, nitrate, sulphate, phosphate and perchlorates were tried to study their effect on the complexation, only the chlorine atoms from the metal salts exhibited their role in the complex as bridging the two square pyramidal units. However, the rest of the counter ions during the complexation escaped from the complex, leading to the formation of the same octahedral complex without any diverse products. The synthesized copper complexes were evaluated for anti-microbial and anti-tuberculosis activity. Anti-tuberculosis activity revealed an MIC value of $1.6 \mu\text{g mL}^{-1}$ for **C3** and $3.125 \mu\text{g mL}^{-1}$ for **C4**, which was almost four and two times more active than standard streptomycin ($6.25 \mu\text{g mL}^{-1}$), and two times more active than and as active as the pyrazinamide and ciprofloxacin ($3.125 \mu\text{g mL}^{-1}$ each) standards, respectively. Also, the ligand **L2H** and all its copper complexes were highly active and even better than the 'Ciprofloxacin' control for the *S. aureus* microorganism, but for *E. coli*, except the **C3** complex, the rest of the compounds demonstrated activities better than the control. **L1H** and both of its complexes were very sensitive to *E. coli* at low concentration of $0.4 \mu\text{g mL}^{-1}$; however, only **C2** was sensitive at $0.8 \mu\text{g mL}^{-1}$ concentration against *S. aureus*. The activities demonstrated by the synthesized compounds are encouraging and illustrate the prospective of these copper complexes as potential chemotherapeutic drugs as anti-microbial and anti-

tubercular agents. However, these results are preliminary in nature, and detailed study of the mechanistic operation of these compounds must be undertaken to expand the efficacy of these as effective metal-based drugs.

ACKNOWLEDGEMENTS

The authors are thankful to USIC, Karnatak University, Dharwad, India, for providing spectral facilities. Recording of NMR from IISc-Bangalore, EPR from SAIF IIT Bombay, biological activity studies from Maratha Mandal's Institute of Dental Science & Research Centre, Belgaum, and SXRD analysis from Mysore University are all gratefully acknowledged. One of the authors (Ganesh S. Hegde) is thankful to the University Grants Commission, New Delhi (U.G.C.) for providing financial assistance under the Minor Research Project program with the UGC approval Letter No. MRP(S)-0475/13-14/KAKA089/UGC-SWRO and M. E. S., M. M. Arts and Science College, Sirsi, Uttara Kannada, Karnataka, India, for the basic research facilities, respectively.

ORCID

Ganesh S. Hegde  <https://orcid.org/0000-0003-4989-2487>
Sandeep P. Netalkar  <https://orcid.org/0000-0003-4187-2123>
Vidyanand K. Revankar  <https://orcid.org/0000-0001-8087-5875>

REFERENCES

- [1] N. P. Hoi, *J. Chem. Soc.* **1953**, 1358.
- [2] S. Pal, *Proc. Indian Acad. Sci. (Chem. Sci.)* **2002**, *114*(4), 417.
- [3] M. C. Rodríguez-Argüelles, S. Mosquera-Vázquez, P. Tourón-Touceda, J. Sanmartín-Matalobos, A. M. Garci-Deibe, M. B. Ferrari, G. Pelosi, C. Pelizzi, F. Zani, *J. Inorg. Biochem.* **2007**, *101*, 138.
- [4] D. S. Kalinowski, P. C. Sharpe, P. V. Bernhardt, D. R. Richardson, *J. Med. Chem.* **2008**, *51*, 331.
- [5] E. W. Ainscough, A. M. Brodie, A. J. Dobbs, J. D. Ranford, J. M. Waters, *Inorg. Chim. Acta* **1998**, *27*, 267.
- [6] J. D. Ranford, J. J. Vital, Y. M. Wang, *Inorg. Chem.* **1998**, *37*, 1223.
- [7] H. A. Offe, W. Siefken, G. Z. Domagk, *Z. Naturforsch.* **1952**, *7B*, 462.
- [8] M. Nandy, D. L. Hughes, G. M. Rosair, R. B. Singh, S. Mitra, *J. Coord. Chem.* **2014**, *67*(20), 3335.
- [9] R. Mezey, I. Máthé, S. Shova, M. N. Grecu, T. Roşu, *Polyhedron* **2015**, (102), 684. <https://doi.org/10.1016/j.poly.2015.10.035>
- [10] S. S. Tajudeen, G. Kannappan, *Ind. J. Adv. Chem. Sci.* **2016**, *4*(1), 40.
- [11] O. V. Dolomanov, L. J. Bourhis, R. J. Gildea, J. A. K. Howard, H. Puschmann, *J. Appl. Cryst.* **2009**, *42*, 339.
- [12] M. C. Burla, R. Caliandro, M. Camalli, B. Carrozzini, G. L. Cascarano, L. De Caro, C. Giacovazzo, G. Polidori, R. Spagna, *J. Appl. Crystallogr.* **2005**, *38*, 381.
- [13] P. W. Betteridge, J. R. Carruthers, R. I. Cooper, K. Prout, D. J. Watkin, *J. Appl. Cryst.* **2003**, *36*, 1487.
- [14] D. J. Watkin, C. K. Prout, L. J. Pearce, *Cameron*, Chemical Crystallography Laboratory, Oxford, England **1996**.
- [15] M. N. Burnett, C. K. Johnson, *ORTEP-III: Oak Ridge Thermal Ellipsoid Plot Program for Crystal Structure Illustrations*, Oak Ridge National Lab, USA: N.p. **1996** <https://doi.org/10.2172/369685>.
- [16] A. Scheurer, P. Mosset, W. Bauer, R. W. Saalfrank, *Eur. J. Org. Chem.* **2001**, *2001*, 3067.
- [17] A. I. Vogel, *Text Book of Practical Organic Chemistry*, 5th ed., Longman, London **1989**.
- [18] V. Sharma, D. K. Mehta, S. Bala, Rina Das, *Int. J. Universal Pharmacy and Bio Sci.* **2013**, *2*(4), 241.
- [19] A. K. Kini, G. S. Hegde, V. K. Revankar, *J. Ind. Coun. Chemists* **2013**, *30*(1 & 2), 181.
- [20] W. J. Geary, *Coord. Chem. Rev.* **1971**, *7*, 81.
- [21] E. A. Mohamed, K. Youness, M. E. Hamidi, *Res. J. Chem. Sci.* **2014**, *4*(10), 72.
- [22] M. V. Angelusiu, S.-F. Barbuceanu, C. Draghici, G. L. Almajan, *Eur. J. Med. Chem.* **2010**, *45*, 2055.
- [23] P. Frohberg, C. Wagner, R. Meier, W. Sippl, *Tetrahedron* **2006**, *62*, 6050.
- [24] P. V. Bernhardt, G. J. Wilson, P. C. Sharpe, D. S. Kalinowski, D. R. Richardson, *J. Biol. Inorg. Chem.* **2008**, *13*, 107. <https://doi.org/10.1007/s00775-007-0300-4>
- [25] F. Krauth, R. Friedemann, H.-H. Ruttinger, P. Frohberg, *ARKIVOC* **2009**, *vii*, 150.
- [26] N. P. Belskaya, W. Dehaen, V. A. Bakulev, ISSN 1551-7012, *ARKIVOC* **2010**, 275.
- [27] R. S. Baligar, V. K. Revankar, *J. Serb. Chem. Soc.* **2006**, *71*, 1301.
- [28] H. M. Dalloul, *ARKIVOC* **2008**, *14*, 234.
- [29] D. L. Pavia, G. M. Lampman, G. S. Kriz, J. R. Vyvyan, *Spectroscopy*, Cengage Learning India Pvt. Ltd., Brooks/Cole **2007** 63.
- [30] G. Quanli, C. Trindle, J. L. Knee, *J. Chem. Phys.* **2012**, *137*, 091101.
- [31] J. Dunkers, E. A. Zarate, H. Ishida, *J. Phys. Chem.* **1996**, *100*, 13 514.
- [32] J. Kelemen, S. Moss, H. Sauter, T. Winkler, *Dyes and Pigm.* **1982**, *3*, 27.
- [33] F. Rahaman, B. H. M. Mruthyunjayaswamy, *Complex Metals* **2014**, *1*(1), 88. <https://doi.org/10.1080/2164232X.2014.889580>
- [34] A. A. Abou-Hussein, W. Linert, *Spectrochim. Acta A Mol. Biomol. Spectrosc.* **2014**, *117*, 763.
- [35] A. M. Hassaanl, M. A. Khalifa, A. K. Shehata, *Bull. Soc. Chim. Belg.* **1995**, *3*, 104.
- [36] M. M. Bekheit, A. R. El-Shobaky, M. T. Gad Allah, *Arab. J. Chem.* **2013**, *10*, S3064. <https://doi.org/10.1016/j.arabj.2013.11.048>
- [37] G. Küçükgülzel, A. Kocatepe, E. D. Clercq, F. Şahin, M. Güllüce, *Eur. J. Med. Chem.* **2006**, *41*, 353.

- [38] K. Hamidian, M. Irandoust, E. Rafiee, M. Joshaghani, Z. *Naturforsch.* **2012**, *67b*, 159.
- [39] G. Yeğiner, M. Gülcan, S. Işık, G. Ö. Ürüt, S. Özdemir, M. Kurtoğlu, *J. Fluoresc.* **2017**, *27*, 2239.
- [40] S. Thakurta, J. Chakraborty, G. Rosair, J. Tercero, M. S. el Fallah, E. Garribba, S. Mitra, *Inorg. Chem.* **2008**, *47*, 6227.
- [41] M. Sebastian, V. Arun, P. P. Robinson, P. Leeju, D. Varghese, *J. Coord. Chem.* **2009**, *63*, 307.
- [42] A. B. P. Lever, *Inorganic Electronic Spectroscopy*, 2nd ed., Elsevier, Amsterdam **1984** 555.
- [43] A. A. G. Tomlinson, B. J. Hathaway, D. E. Billing, D. Nichollas, *J. Chem. Soc. A* **1969**, 65.
- [44] P. Chaudhuri, K. Oder, *J. Chem. Soc. Dalton Trans.* **1990**, 1597.
- [45] H. Okawa, M. Tadokoro, Y. Aratake, M. Ohbaand, D. E. Fenton, *J. Chem. Soc. Dalton Trans.* **1993**, 253.
- [46] M. Handa, T. Idehara, K. Nakano, K. Kasuga, M. Mikuriya, N. Matsumoto, M. Kodera, S. Kida, *Bull. Chem. Soc. Jpn.* **1992**, *65*, 3241.
- [47] R. S. Himmelwright, N. C. Eickman, E. I. Solomon, *J. Am. Chem. Soc.* **1979**, *101*, 1576.
- [48] H. Adams, D. E. Fenton, S. R. Haque, S. E. Spey, *J. Chem. Soc. Dalton Trans.* **2000**, 1849.
- [49] S. Okawa, Y. Kida, T. Muto, Tokii, *Bull. Chem. Soc. Jpn.* **1972**, *45*, 2480.
- [50] S. M. Annigeri, M. P. Sathisha, V. K. Revankar, *Trans. Met. Chem.* **2007**, *32*, 81.
- [51] D. Kivelson, R. Neiman, *J. Chem. Phys.* **1961**, *35*, 149.
- [52] S. Roy, P. Mitra, A. K. Patra, *Inorg. Chim. Acta* **2011**, *370*, 247.
- [53] S. Mukherjee, C. Basu, S. Chowdhury, A. P. Chattopadhyay, A. Ghorai, U. Ghosh, H. Stoeckli-Evans, *Inorg. Chim. Acta* **2010**, *363*, 2752.
- [54] P. P. Netalkar, S. P. Netalkar, V. K. Revankar, *Polyhedron* **2015**, *(100)*, 215.
- [55] A. K. Patra, R. Mukherjee, *Inorg. Chem.* **1999**, *38*, 1388.
- [56] M. Schwalve, Goodwin, *Antimicrobial Susceptibility Testing Protocols*, CRC Press, Boca Raton, FL **2007**.
- [57] M. C. S. Lourenco, M. V. N. D'Souza, A. C. Pinheiro, M. L. Ferreira, R. S. B. Goncalves, T. C. M. Nogueira, M. A. Peralta, *ARKIVOC* **2007**, *15*, 181.

SUPPORTING INFORMATION

Additional supporting information may be found online in the Supporting Information section at the end of the article.

How to cite this article: Hegde GS, Netalkar SP, Revankar VK. Copper (II) complexes of 3,5-di-*tert*-butyl-2-hydroxybenzoylhydrazones of 2-formylpyridine and 2-acetylpyridine, with tautomeric azine-scaffold-based architecture: Synthesis, crystal structures, the effect of counteranions on complexation, and their anti-microbial and anti-tuberculosis evaluation. *Appl Organometal Chem.* 2019;33:e4840. <https://doi.org/10.1002/aoc.4840>